JCTC Journal of Chemical Theory and Computation

Article

pubs.acs.org/JCTC

Benchmarking the Fundamental Electronic Properties of small TiO_2 Nanoclusters by *GW* and Coupled Cluster Theory Calculations

Enrico Berardo,[†,‡] Ferdinand Kaplan,[§] Kiran Bhaskaran-Nair,[∥] William A. Shelton,[∥] Michiel J. van Setten,[*,⊥] Karol Kowalski,[*,#] and Martijn A. Zwijnenburg[*,‡]

[†]Department of Chemistry, Imperial College London, South Kensington, London SW7 2AZ, United Kingdom

[‡]Department of Chemistry, University College London, 20 Gordon Street, London WC1H 0AJ, United Kingdom

[§]Institute of Nanotechnology, Karlsruhe Institute of Technology, Campus North, D-76344 Karlsruhe, Germany

[∥]Cain Department of Chemical Engineering, Louisiana State University, Baton Rouge, Louisiana 70803, United States

[⊥]Nanoscopic Physics, Institute of Condensed Matter and Nanosciences, Université Catholique de Louvain, 1348 Louvain-la-Neuve, Belgium

[#]William R. Wiley Environmental Molecular Science Laboratory, Battelle, Pacific Northwest National Laboratory, K8-91, P. O. Box 999, Richland, Washington 99352, United States

Supporting Information

ABSTRACT: We study the vertical and adiabatic ionization potentials and electron affinities of bare and hydroxylated TiO_2 nanoclusters, as well as their fundamental gap and exciton binding energy values, to understand how the clusters' electronic properties change as a function of size and hydroxylation. In addition, we have employed a range of many-body methods; including G_0W_0, qs*GW*, EA/IP-EOM-CCSD, and DFT (B3LYP, PBE), to compare the performance and predictions of the different classes of methods. We demonstrate that, for bare clusters, all many-body methods predict the same trend with cluster size. The highest occupied and lowest unoccupied DFT orbitals follow the same trends as the electron affinity and ionization potentials predicted by the many-body methods, but are generally far too shallow and deep respectively in absolute terms. In contrast, the ΔDFT method is found to yield values in the correct energy window. However, its predictions depend upon the functional used and do not necessarily follow trends based on the many-body methods. Adiabatic potentials are predicted to be similar to their vertical counterparts and holes found to be trapped more strongly than excess electrons. The effect of hydroxylation on the clusters is to open up both the optical and fundamental gap. Finally, a simple microscopic explanation for the observed trends with cluster size and upon hydroxylation is proposed in terms of the onsite electrostatic potential.

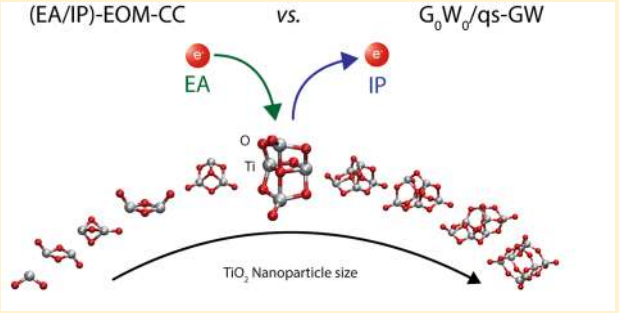

INTRODUCTION

Titanium dioxide (TiO_2) nanostructures are key components of many[1−3] advanced technological products and processes, for example as photocatalysts for water and air purification[4] and photocatalytic water splitting,[5−11] as semiconductors in dye-sensitized solar cells[12,13] and as photocatalytic and super-hydrophilic coatings for self-cleaning windows.[14−16] All these applications depend on a combination of the wettability of TiO_2 by water or other polar solvents, its chemical and mechanical stability in the presence of water and illumination, and the specific optical and/or electronic properties of the TiO_2 nanostructures. TiO_2 is also the archetypal model system for oxide semiconductors where a large amount of fundamental experimental[17−19] and computational[20−59] studies on the optical, electronic, and photocatalytic properties of both bulk and nanostructured TiO_2 have been performed.

Key properties relevant for understanding the optical and electronic properties of TiO_2 nanostructures and materials in general[60] are (i) the fundamental gap (ΔE_f, often referred to as the band gap for crystalline solids), (ii) the optical gap or absorption onset (ΔE_0), (iii) the exciton binding energy (EBE), and (iv) their ionization potential (IP) and electron affinity (EA); see Figures 1 and 2.

The optical gap is the energy above which a system starts absorbing light and singlet excitons are formed, while the fundamental gap is the energy required to make pairs of free charge carriers. The exciton is a bound state of an excited electron in the conduction band and a hole in the valence band, in which the excited electron and hole are attracted to each other by their opposite charge. Triplet excitons can be formed

Received: May 24, 2017
Published: June 19, 2017

DOI: 10.1021/acs.jctc.7b00538
J. Chem. Theory Comput. 2017, 13, 3814−3828

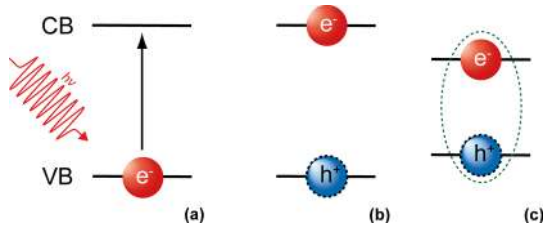

Figure 1. Cartoon representing the excitation process taking place in a material, where the absorption of a photon causes (a) the excitation of an electron to the conduction band (CB), (b) coupled generation of a hole in the valence band (VB), and (c) formation of an electron−hole pair (exciton) bound through their mutual Coulomb interaction.

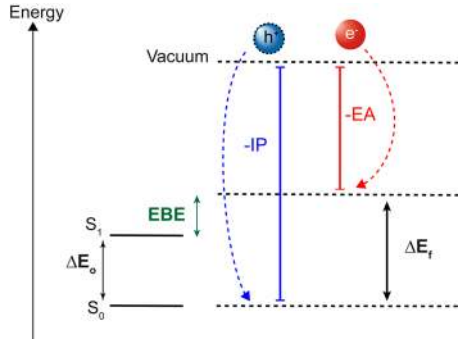

Figure 2. Cartoon illustrating the fundamental gap (ΔE_f), the optical gap or absorption onset (ΔE_o), and the exciton binding energy (EBE), the difference between a materials' ΔE_f and ΔE_o, as well as the ionization potential (IP) and electron affinity (EA) associated with the free hole and free electron, respectively.

from their singlet counterparts through intersystem crossing mediated by spin−orbit coupling but are not directly created upon light absorption due to the spin forbidden nature of the underlying transition. The exciton binding energy is the energy needed to separate the electron and hole (i.e., to convert them to free charge carriers). For systems that lack strict periodicity (i.e., clusters, polymers, and so on) the difference between the fundamental gap and optical gap is purely a measure of the extent to which singlet excitons are energetically stabilized with respect to free charge carriers due to the electrostatic interaction. Systems are inherently transparent to light below the optical gap and below the fundamental gap cannot carry a photocurrent. The energies of the valence and conduction bands relative to the vacuum level and the charge carriers in them correspond to the negative of the ionization potential (IP, the energetic cost of removing an electron and forming a cation) and electron affinity (EA, the energy released upon adding an electron and forming an anion). All these properties can in principle couple with phonons, i.e., nuclear degrees of freedom. For example, the experimental onset of light absorption will be slightly red-shifted with respect of the vertical optical gap due to contributions of (nonvertical) vibronic transitions. Similarly, while the lowest energy peak maxima in a nonvibrationally resolved photoelectron spectrum will approximately coincide with the vertical IP, the onset of electron emission is linked to the adiabatic IP, which includes the effect of nuclear relaxation after removal of an electron. Here, in analogy with the typical theoretical convention for solids, we will concentrate on vertical properties, but for selected clusters, we also explicitly explore the effect of nuclear relaxation.

The majority of computational studies on TiO_2 nanostructures are based on density functional theory (DFT)[61] and methods such as TD-DFT and *GW*, which are built on top of DFT. Specifically, the optical and/or fundamental gap within DFT is approximated by the difference between the highest occupied and lowest unoccupied (generalized) Kohn−Sham (KS) orbitals (Kohn−Sham (KS-) gap).[62] Other DFT studies[25,31,52,53,57] calculate the vertical and/or adiabatic electron affinity (EA) and ionization potential (IP) of nanostructures explicitly using a ΔSCF (ΔDFT) approach[63,64] and obtain the fundamental gap by taking the difference between the vertical EA and IP. Similar studies[26,31,44,45,51,56] use

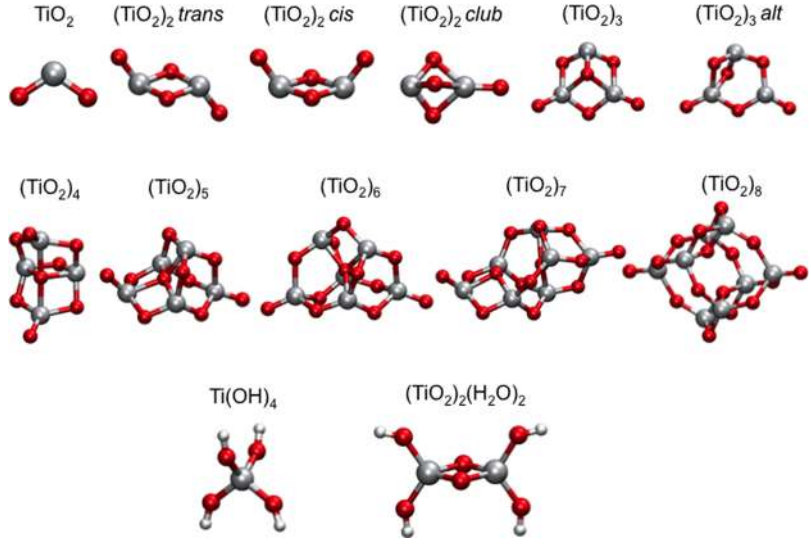

Figure 3. B3LYP/def2-TZVP optimized structures of the bare and hydroxylated TiO_2 nanoparticles studied. The $(TiO_2)_2$ trans, $(TiO_2)_3$, $(TiO_2)_4$, $(TiO_2)_5$, $(TiO_2)_6$, $(TiO_2)_7$, and $(TiO_2)_8$ nanoclusters correspond to global minima candidate structures for that number of TiO_2 units, whereas $(TiO_2)_2$ cis, $(TiO_2)_2$ club, and $(TiO_2)_3$ alt represent higher lying minima. The hydroxylated $(TiO_2)_2(H_2O)_2$ cluster was manually constructed by adding -H and -OH groups to the bare $(TiO_2)_2$ global minimum candidate. Titanium, oxygen, and hydrogen atoms are shown as gray, red, and white spheres, respectively.

DOI: 10.1021/acs.jctc.7b00538
J. Chem. Theory Comput. 2017, 13, 3814−3828

time-dependent DFT[65] (TD-DFT) to calculate the optical gap as the lowest energy excited state of the nanostructure. Finally, there are studies[27,31,35,38,40,44−46,48,55,58] that go beyond DFT either using many-body perturbation theory; Green's function based *GW* theory for the fundamental gap,[66−68] and *GW* in combination with solving the Bethe−Salpeter equation (BSE) for the optical gap,[69] as well as quantum chemistry methods.[70−73]

The predominance of calculations based on (TD-)DFT is directly linked to the very favorable computational scaling with system size relative to the inherently more accurate alternatives, allowing for calculations on true nanosized systems. The drawback of (TD-)DFT, however, is the need in practice to use approximate exchange-correlation (XC) density functionals, as the functional form of the exact density functional is not known. The results obtained with (TD-)DFT are hence to a degree functionally dependent and ideally need to be validated by comparison with experimental or computational benchmark data.

Here we build further on our previous efforts[40,44,45] to generate benchmark data for the optical gap and photoluminescence energy of small TiO_2 model nanoclusters using equation-of-motion coupled-cluster (EOM-CC) theory. We predict vertical and adiabatic −EA and −IP values and vertical fundamental gap values and exciton binding energies for the same model clusters using both Green's function based methods: G_0W_0,[66−68] quasi-particle self-consistent qs*GW*,[74−77] and coupled-cluster[70] (CC) theory based approaches: ΔCC and EA/IP-EOM-CC.[78] Such nanoclusters, see Figure 3, are arguably smaller than the nanostructures encountered experimentally in all but mass spectrometry type of experiments[17,18,79,80] but can be conveniently studied by both DFT and *GW*/CC methods. We also compare the results of different *GW* and CC methods, as well as their convergence with increasing basis-set size, and comment on the suitability of each to describe TiO_2 clusters. In the case of EA we also compare our G_0W_0 and EA-EOM-CCSD predictions to experimental data. Finally, we consider the effect of hydroxylation on the fundamental gap and exciton binding energy of TiO_2 clusters.

GW and CC Methods. *G_0W_0 and qsGW.* The central object in the *GW* formalism is the causal Green's function *G*. Formally it is obtained from the Dyson equation

$$G(E) = (E - H_{\mathrm{H}}[G] - \sum[G])^{-1} \tag{1}$$

where H_{H} is a noninteracting reference Hamiltonian, i.e., the Hartree Hamiltonian, and Σ is the so-called self-energy. In the *GW* approximation the self-energy is taken as the first-order expansion of the self-energy in terms of the screened Coulomb interaction *W*:Σ = *GW*. The zero-order expansion corresponds to Hartree−Fock (HF) theory. In general Σ is nonhermitian and energy-dependent.

In the quasi-particle approximation the Green's function is expanded in terms of quasi-particles ψ^{QS} with eigenvalues $\varepsilon^{\mathrm{QS}}$:

$$G(\mathbf{r}, \mathbf{r}', \mathbf{E}) = \sum_n \frac{\psi_n^{\mathrm{QP}}(\mathbf{r})\,\overline{\psi_n^{\mathrm{QP}}}(\mathbf{r}')}{E - \varepsilon_n^{\mathrm{QP}} + i\mathrm{sign}(\varepsilon_n^{\mathrm{QP}} - \mu)} \tag{2}$$

The sum runs over all occupied and unoccupied single-particle states; μ is the Fermi energy. In this approach the Green's function hence keeps the analytical form of a noninteracting Green's function. In the G_0W_0 approach, the ionization energies and electron affinities are obtained from the quasi-particle energies, $\varepsilon^{\mathrm{QP}}$, which are evaluated as a first-order perturbative correction to a set of noninteracting single-particle states. In practice these are usually the Kohn−Sham orbitals, ψ^{KS}, with eigenvalues, $\varepsilon^{\mathrm{KS}}$:

$$\varepsilon_n^{\mathrm{QP}} = \varepsilon_n^{\mathrm{KS}} + \langle \psi_n^{\mathrm{KS}} | \Sigma(\varepsilon_n^{\mathrm{QP}}) - \mathrm{V}^{\mathrm{XC}} | \psi_n^{\mathrm{KS}} \rangle \tag{3}$$

Although eq 3 is solved iteratively for $\varepsilon^{\mathrm{QP}}$, due to its perturbative nature the final $\varepsilon^{\mathrm{QP}}$ values still depend on the starting point, that is, on the (arbitrary) set of eigenvalues $\varepsilon^{\mathrm{KS}}$ and orbitals ψ^{KS}. In this work we use the B3LYP XC functional[81,82] to generate the initial set of KS eigenvalues and orbitals for our G_0W_0 calculations.[77]

In qs*GW* self-consistency is reached at the level of the quasi-particle orbitals and energies.[74−76] In contrast to G_0W_0 where only the diagonal matrix elements of the self-energy are needed, in qs*GW* also the off-diagonal matrix elements are required. To lift the nonhermiticity of Σ and obtain a single set of orthonormal quasi-particle states, the exact self-energy matrix elements are replaced by

$$\hat{\Sigma}_{nn'} = \frac{1}{2}(\Sigma_{nn'}(\varepsilon_n) + \Sigma_{n'n}(\varepsilon_{n'})) \tag{4}$$

The solution of eq 1 is organized in an iterative scheme starting from the KS initialization. The QP orbitals of the $(i + 1)$th iteration $\psi^{(i+1)}(r)$ are expressed in the reference orbitals of the previous iteration, defining the coefficient matrix **A**:

$$\psi_n^{(i+1)}(\mathbf{r}) = \sum_{n'} A_{nn'}^{(i+1)}\, \psi_{nn'}^{(i)}(\mathbf{r}) \tag{5}$$

In this reference basis eq 1 becomes an eigenvalue problem:

$$\sum_{n''} A_{n'n''}^{(i+1)}[\int \mathrm{d}\mathbf{r} \int \mathrm{d}\mathbf{r}'\, \psi_n^{(i)}(\mathbf{r})(H_{\mathrm{H}}[G^{(i)}]\delta(\mathbf{r} - \mathbf{r}') + \hat{\Sigma}[G^{(i)}](\mathbf{r}, \mathbf{r}'))\psi_{n''}^{(i)}(\mathbf{r}')] = \varepsilon_{n'}^{(i+1)} A_{n'n}^{(i+1)} \tag{6}$$

which yields updated $\varepsilon_n^{(i+1)}$ and $A_{n'n}^{(i+1)}$, where the latter are used to construct new orbitals $\psi_{n'}^{(i+1)}(\mathbf{r})$.

The final result of eq 6 has been shown to be independent of the starting point,[76] but both the stability of the iterative cycle and the rate of convergence can be greatly improved by using an optimal starting point. Hybrid functionals such as the B3LYP XC functional are known to give good starting points. Moreover, the actual implementation contains a linear mixing scheme in eq 6 to improve stability.

ΔCC and EA/IP-EOM-CC. In the EA/IP extension of the equation-of-motion CC approach[78] the *k*th wave functions of *N* ± 1 particle systems are represented in the form of the EOM-CC Ansatz

$$|\Psi_k\rangle = R(k)\, \mathrm{e}^T |\Phi\rangle \tag{7}$$

where $|\Phi\rangle$, *T*, and $R(k)$ are the reference Slater determinant, typically from a previous Hartree−Fock calculation, the cluster operator for the *N*-electron system, and the excitation operator, respectively. In the rudimentary EA/IP-EOM-CCSD approximations the IP and EA excitation operators, $R^{\mathrm{IP}}(k)$ and $R^{\mathrm{EA}}(k)$ are represented as

$$R^{\mathrm{IP}}(k) = \sum_i r^i(k) a_i \sum_{i<j;a} r^{ij}{}_a(k) a_a^+ a_j a_i \tag{8}$$

$$R^{\mathrm{EA}}(k) = \sum_a r_a(k) a_a^+ + \sum_{i;a<b} r^i{}_{ab}(k) a_a^+ a_b^+ a_i \tag{9}$$

DOI: 10.1021/acs.jctc.7b00538
J. Chem. Theory Comput. 2017, 13, 3814−3828

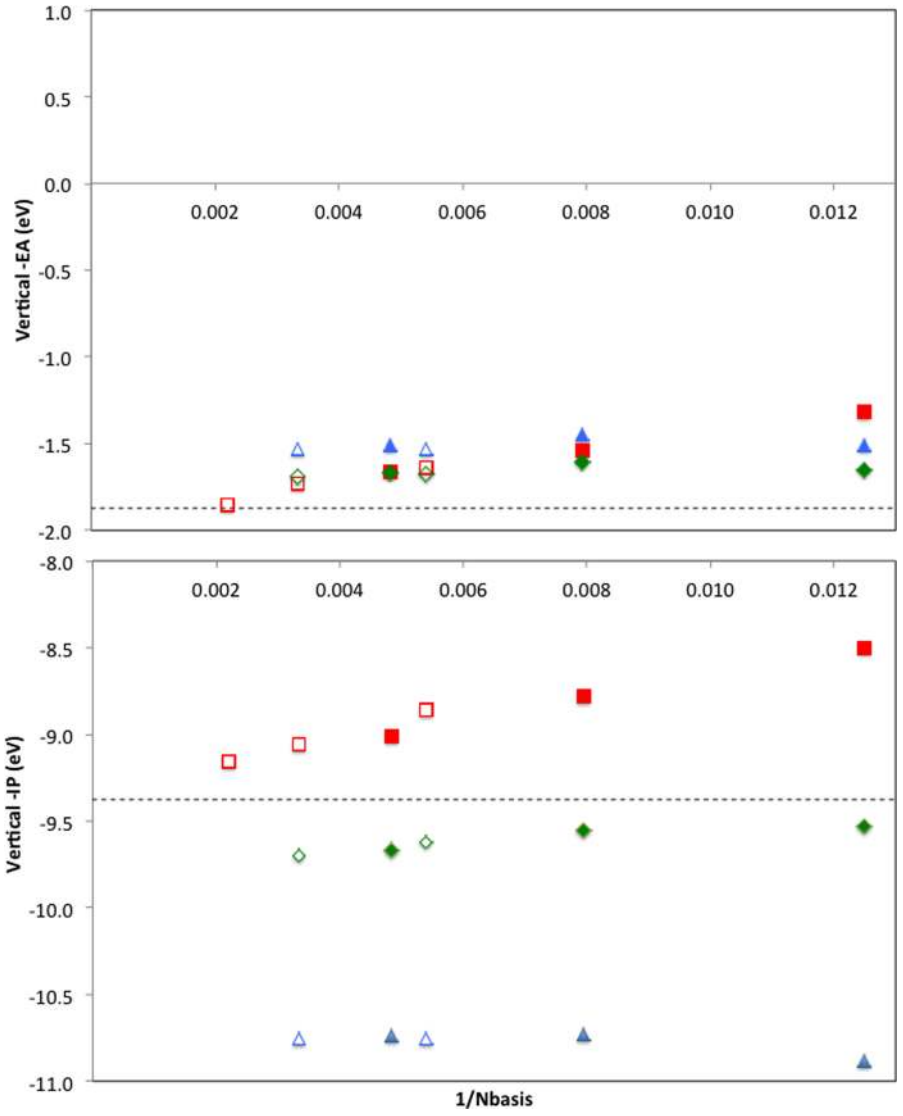

Figure 4. Vertical −IP (bottom panel) and −EA (top panel) values of the TiO2 molecule calculated with the different methods and different basis sets as a function of the number of basis functions in the basis set (Nbasis). Blue triangles are ΔB3LYP results; red squares are calculated with G_0W_0, and green diamonds, with EA/IP-EOM-CCSD. Filled symbols correspond to values calculated with basis sets from the Ahlrichs family and open symbols from the Dunning family. The dashed lines correspond to the G_0W_0 values extrapolated to the complete basis-set limit using approach **A** (data shown in Table 1). All G_0W_0 calculations were started from a DFT calculation with the B3LYP XC functional. All values are in electronvolts.

where a_p and a^+_p are the annihilation and creation operators for the electron in pth spin−orbital and following the convention labeling occupied orbitals with i and j and unoccupied orbitals with a and b. The EOM-CCSD ionization potentials, electron affinities, and corresponding excitation operators are obtained by diagonalizing a similarity transformed Hamiltonian in normal-product form $\bar{H}_N$ (see ref 78 for details) in the $N \pm 1$ particle subspaces spanned by single and double excitations; i.e.,

$$\bar{H}_N R(k)|\Phi\rangle = \omega(k)\, R(k)|\Phi\rangle \tag{10}$$

where the $\omega(k)$ values correspond either to ionization potentials or electron affinities.

Contrasting Both Approaches. While both classes of methods have rather different starting points and are described in terms of different mathematical objects, they are also closely interrelated. For example, the fully interacting CC Green's function can in principle be obtained from the CC wave function and then be used to extract the CC self-energy Σ through the Dyson equations. Indeed, the EA/IP-EOM-CCSD methods used here are closely related to the Green's function−CCSD method[83−90] explicitly developed for this purpose, which utilizes the bivariational formulation of the CC formalism. The matrix elements of the CC Green function matrix, G_{pq}, take the following form:

$$G_{pq}(\omega) = \langle\Phi|(1+\Lambda)\,\overline{a_q^+} X_p(\omega)|\Phi\rangle + \langle\Phi|(1+\Lambda)\,\overline{a}_p Y_q(\omega)|\Phi\rangle \tag{11}$$

where $\langle\Phi|(1+\Lambda)$ is the left eigenvector of the similarity transformed Hamiltonian $\bar{H} = e^{-T} H e^{T}$ and $\overline{a}^+_q$ and $\overline{a}_p$ are the similarity transformed creation and annihilation operators a_q^+ and a_p; i.e.,

$$\overline{a_q^+} = e^{-T} a_q^+ e^{T} \tag{12}$$

$$\overline{a}_p = e^{-T} a_p e^{T} \tag{13}$$

DOI: 10.1021/acs.jctc.7b00538
J. Chem. Theory Comput. 2017, 13, 3814−3828

The $X_p(\omega)$ and $Y_q(\omega)$ operators in eq 11 are the ionization potential/electron affinity type operators which assume singular values for ω values corresponding to the EA/IP-EOMCC eigenvalues ω_k. In other words, all poles of the CCSD Green's function correspond to the eigenvalues of the IP/EA-EOM-CCSD equations.

Both classes of many-body methods can be systematically improved. By adding higher order excitations to the EA/IP-EOM-CC excitation operators, in analogy to the standard EOM-CC formulations, one can define a hierarchy of approximations converging to the full configuration interaction limit once all possible excitations are included. Similarly, *GW* can be improved upon by going beyond the zero- and first-order terms of the self-energy expansion. In practice this knowledge is of limited use in predicting the relative accuracy of qs*GW* and EA/IP-EOM-CCSD for systems of interest. G_0W_0, being an approximation to qs*GW*, should be less accurate than qs*GW*, but the difference between the two methods can be minimized by choosing an optimal starting point.[76,91]

Computational Details. The (vertical) ionization potential, electron affinity, fundamental gap, optical gap, and exciton binding energy were calculated for a series of $(TiO_2)_n$ clusters and two $(TiO_2)_n(H_2O)_m$ clusters (see Figure 3). The structures of the clusters discussed here were taken from our previous studies[40,44,45] and were originally obtained through global optimization,[20,26,38,92] with the exception of the hydrated structures which were constructed manually by adding -H and -OH groups to the bare global minima candidate structures.[44] In our earlier works[40,44,45] the xyz coordinates of all the clusters were optimized using a combination of the B3LYP[81,82] hybrid XC functional and the def2-TZVP[93,94] basis set, using Turbomole 6.6.[95,96] As discussed in the Introduction, IP and EA of the clusters were calculated using a range of approaches: from taking the DFT KS orbital energies to using the ΔDFT, G_0W_0, qs*GW*, ΔCCSD, ΔCCSD(T), ΔCCSDT, and EA/IP-EOM-CCSD methods. The optical gap of selected clusters was approximated as the lowest vertical singlet excitation energy and calculated using EOM-CCSD. All the coupled cluster calculations, for reasons of computational tractability, employed the frozen core approximation where only the valence electrons are correlated. The (Δ)DFT and *GW* calculations were performed in Turbomole 6.6,[95,96] the qsGW calculations in a locally modified version of Turbomole 7.0,[76] while the coupled cluster calculations used NWChem 6.6.[97] All these calculations, finally, employed basis sets from the Ahlrichs[93,94,98] (def2-SVPD, def2-TZVPP, and def2-QZVPP) and Dunning[99,100] (aug-cc-pVTZ, aug-cc-pVQZ, and aug-cc-pV5Z) families of Gaussian basis sets.

RESULTS AND DISCUSSION

Effect of Basis-Set Size. We analyze the effect of basis-set size on the predictions of vertical −IP and −EA values by the ΔB3LYP, G_0W_0, and EA/IP-EOM-CCSD methods through a comparison of results for the TiO_2 molecule calculated with a range of basis sets from Ahlrichs and Dunning basis-sets families, where possible, extrapolating the results to the complete basis-set limit. Figure 4 shows the predicted vertical −IP and −EA values calculated with ΔB3LYP, G_0W_0 and EA/IP-EOM-CCSD and the Ahlrichs and Dunning basis-set families plotted against the number of basis functions in the basis set (Nbasis). Table S1 in the Supporting Information presents the same information in table form. Concentrating first on the results obtained with basis sets from the Ahlrichs family (filled symbols), the vertical −IP and −EA values are generally predicted to become more negative with increasing basis-set size, except for the case of ΔB3LYP, where −IP and −EA do not really change with basis-set size. Moreover, the change with basis set is generally larger for −IP than in −EA, at least in absolute terms. In addition, it appears that G_0W_0 shows a much stronger dependence on the size of the basis set used than either EA/IP-EOM-CCSD or ΔB3LYP. Contrasting the results obtained with basis sets from the Ahlrichs and Dunning families (the open symbols), it seems that when comparing basis sets of the same cardinality (e.g., def2-TZVP and aug-cc-pVTZ), the Dunning basis sets always yield slightly more negative −IP and −EA values, in line with the fact that the latter always contain more primitive basis functions, as well as proper diffuse functions.

Table 1 provides the extrapolations of the G_0W_0 −IP and −EA values to the complete basis-set limit (CBS). Three different extrapolation methods were tried: (**A**) a linear extrapolation of −IP and −EA as a function of one over the number of basis functions (Nbasis) in each of the basis sets, i.e., $a + b/\text{Nbasis}$; (**B**) a linear extrapolation of −IP and −EA as a function of one over the cube of the cardinality (CN) of each of the basis sets, i.e., $a + b/\text{CN}^3$; and (**C**) an exponential extrapolation as a function of CN, i.e., $a + b\exp(c(\text{CN}))$. All three extrapolation methods give similar results for −EA in the CBS limit, while for −IP in the CBS limit **A** yields a more negative value than either **B** or **C**. Regardless, the results of the extrapolation suggest that, as expected from the results in Figure 4, G_0W_0 even for triple-ζ basis sets yields −EA values that deviate 0.5−0.6 eV and −IP values that differ by 0.2−0.3 eV from the CBS limit. Comparing these deviations to those found in a recent work studying a selection of 100 molecules with G_0W_0,[101] it appears that in the case of TiO_2 G_0W_0 performs worse than average for −IP and better than average for −EA.

Table 1. G_0W_0 Vertical −IP and −EA Values of the TiO_2 Molecule Extrapolated to the CBS Limit by the Three Different Approaches Discussed in Text, as Well as Values of the Square of the Correlation Coefficient (r^2) for the Fits Underlying the Extrapolation

	G_0W_0		r^2	
	−VIP	−VEA	−VIP	−VEA
A	−9.38	−1.87	0.9986	0.9998
B	−9.24	−1.81	0.9959	0.9868
C	−9.25	−1.85	0.9983	0.9994

We cannot perform the same extrapolation for EA/IP-EOM-CCSD, due to linear dependency difficulties when solving the EA/IP-EOM-CCSD equations for the largest of the Dunning family basis sets. However, as discussed above, the data in Figure 4 and Table S1 show that the EA/IP-EOM-CCSD −IP and −EA values vary much less with increasing basis-set size than those obtained with G_0W_0, suggesting that the deviation between triple-ζ (and quadruple-ζ) basis set and CBS limit values for EA/IP-EOM-CCSD might be smaller than for G_0W_0. This weaker effect of basis-set size is in line with previous benchmark EA/IP-EOM-CCSD calculations for the C_2 and F_2 molecules.[78] For ΔB3LYP, not surprisingly, the results are not very sensitive to the basis-set size beyond triple-ζ basis sets.

DOI: 10.1021/acs.jctc.7b00538
J. Chem. Theory Comput. 2017, 13, 3814−3828

Table 2. Vertical −IP and −EA Values of TiO_2 Nanoclusters Calculated for the Different DFT and *GW* Methods and def2-TZVPP and aug-cc-pVTZ Basis Set[a]

	KS-B3LYP		ΔB3LYP		G_0W_0		qs*GW*	
	−VIP	−VEA	−VIP	−VEA	−VIP	−VEA	−VIP	−VEA
1	−7.00	−3.19	−10.73	−1.45	−8.78	−1.54	−9.96	−1.30
					−8.86	*−1.64*		
2 trans	−8.03	−3.06	−10.66	−1.46	−9.32	−1.39	−10.66	−1.05
					−9.53	*−1.50*		
2 cis	−7.71	−3.27	−10.10	−1.69	−9.13	−1.68	−10.31	−1.39
					−9.21	*−1.78*		
2 club	−7.51	−3.44	−10.46	−1.80	−8.83	−1.84	−9.98	−1.59
					−8.90	*−1.92*		
3	−7.82	−4.16	−9.74	−2.56	−9.12	−2.67		

[a]Values obtainedusing the aug-cc-pVTZ basis-set highlighted in italics. G_0W_0 and qs*GW* calculations started from a DFT calculation with the B3LYP XC functional. Corresponding literature G_0W_0 −VEA values for the relevant $(TiO_2)_2$ and $(TiO_2)_3$ clusters from Marom and co-workers are −1.34, −1.62, −1.92, and −2.75 eV, respectively.[38] All values in electronvolts.

Table 3. Vertical −IP and −EA Values of TiO_2 Nanoclusters Calculated for the Different Coupled-Cluster Methods and the def2-TZVPPP and aug-cc-pVTZ Basis Sets[a]

	EOM-CCSD		ΔCCSD		ΔCCSD(T)		ΔCCSDT	
	−VIP	−VEA	−VIP	−VEA	−VIP	−VEA	−VIP	−VEA
1	−9.55	−1.61	−9.53	−1.47	−9.52	−1.35	−9.52	−1.36
	−9.62	*−1.68*	*−9.60*	*−1.56*	*−9.60*	*−1.46*	*−9.60*	*−1.46*
2 trans	−10.39	−1.32	−10.67	−1.16	−10.53	−1.10		
	−10.39	*−1.32*	−10.73	*−1.25*	*−10.62*	*−1.18*		
2 cis	−10.01	−1.62	−10.67	−1.40	−10.05	−1.44		
	−10.07	*−1.69*	*−10.73*	*−1.49*	*−10.13*	*−1.53*		
2 club	−9.68	−1.89	−10.71	−1.80	−10.71	−1.61		
	−9.74	*−1.93*	*−10.77*	*−1.85*	*−10.79*	*−1.68*		
3	−10.11	−2.64	−10.12	−2.59	−9.97	−2.32		
	−10.14	*−2.66*	*−10.17*	*−2.64*	*−10.03*	*−2.37*		

[a]Values obtained using the aug-cc-pVTZ basis-set highlighted in italics. All values are in electronvolts.

For all methods, the effect of basis-set size on the predicted fundamental gap, discussed in more detail below, is much smaller than on the individual vertical −IP and −EA values. For example, for G_0W_0 the fundamental gap changes only from 7.2 to 7.3 eV when going from the def2-SVPD to the aug-ccp-pV5Z basis set, where the latter, depending on the extrapolation method used, is approximately 0.1−0.2 eV from the extrapolated fundamental gap in the CBS limit of 7.4−7.5 eV. This much smaller change of the fundamental gap with basis-set size than in the constituting vertical −IP and −EA values is due to both displaying, as discussed above, large changes in the same negative direction.

For reasons of computational tractability, we limit ourselves in the remainder of this work to calculations using the def2-SVPD, def2-TZVPP and aug-cc-pVTZ basis sets. This might mean that our results for certain methods, e.g., G_0W_0, deviate in terms of absolute values from those at the basis-set limit, but we expect that trends will remain the same.

Comparing G_0W_0 and qs*GW*. Table 2 compares the vertical −IP and −EA values of the TiO_2 molecule and $(TiO_2)_2$ and $(TiO_2)_3$ clusters obtained with DFT, G_0W_0 and qs*GW*. Concentrating on the latter two methods, G_0W_0 and qs*GW* appear to predict the same trends, which are discussed below in more detail, but qs*GW* predicts −IP values that are consistently deeper, by ∼1 eV, and −EA values that are consistently shallower, by ∼0.3 eV, than G_0W_0. This shift, at least for the −IP values, is similar in magnitude and direction to those previously observed when applying G_0W_0 and qs*GW* to a range of simple organic and main-group molecules.[76] Use of aug-cc-pVTZ rather than def2-TZVPP in the G_0W_0 calculations gives, in line with what was discussed above for the TiO_2 molecule, very similar results. The effect of adding diffuse functions hence appears small.

The −EA values of some of the small TiO_2 clusters were previously studied using G_0W_0 by Marom and co-workers.[38] Our G_0W_0/B3LYP/def2-TZVPP and G_0W_0/B3LYP/aug-cc-pVTZ −EA values in Table 2 for the different isomers of $(TiO_2)_2$ and the $(TiO_2)_3$ global minimum candidate lie within 0.1 and 0.2 eV, respectively of Marom and co-workers' G_0W_0/PBEh values obtained using FHI-Aims and large (tier 4) numerical basis sets. The minor differences between our and their values are probably due to differences in the basis-set quality and the density functional, B3LYP vs PBEh, used to obtain the starting eigenvalues and eigenvectors.

As an aside, comparing the def2-TZVPP and def2-SVPD ΔB3LYP results in Tables 2 and S2, it is clear that while, as discussed above, the ΔB3LYP results in general have a weak dependency on the basis-set size, the predictions for the −IP values of the club isomer of $(TiO_2)_2$ and the $(TiO_2)_3$ global minimum candidate structure are significantly different. A comparison of the spin population for the cation structures in these cases suggests that this is the result of the SCF with the two basis sets converging to solutions with different distributions of the unpaired spin over the clusters.

Comparing EOM-CC and ΔCC. Table 3 compares the vertical −IP and −EA values of the TiO_2 molecule, the different

DOI: 10.1021/acs.jctc.7b00538
J. Chem. Theory Comput. 2017, 13, 3814−3828

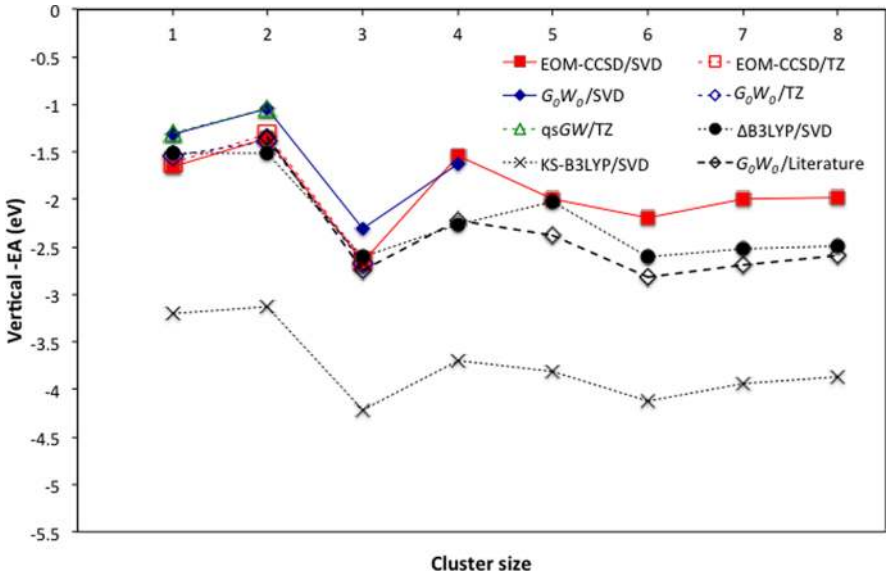

Figure 5. Trend in the vertical −EA values of the TiO_2 global minimum candidate structures with the number of TiO_2 units in a cluster predicted by G_oW_o, qs*GW*, EA/IP-EOM-CCSD, ΔB3LYP, and KS-B3LYP using the def2-SVPD (SVD) and def2-TZVPP (TZ) basis sets, as well as literature G_oW_o values from Marom and co-workers.[38] ΔPBE results can be found in Figure S1 in the Supporting Information.

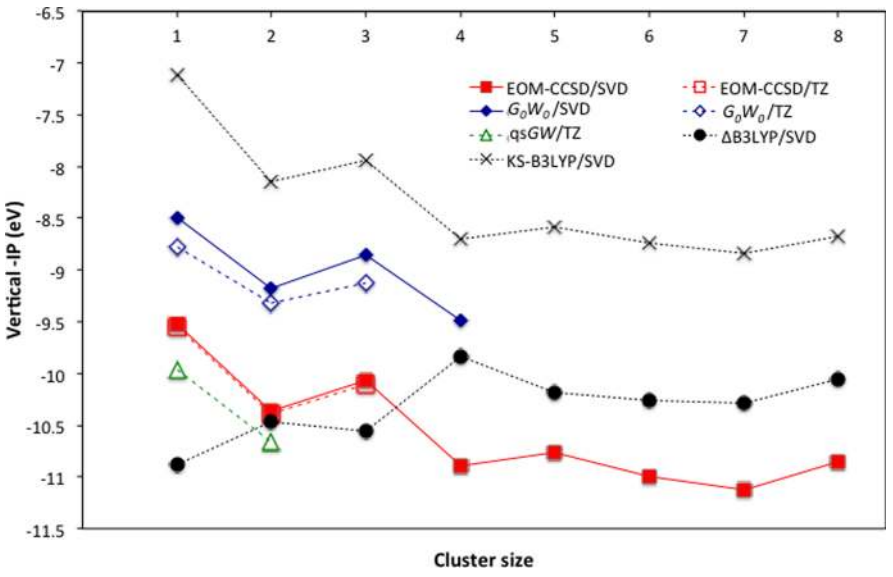

Figure 6. Trend in the vertical −IP values of the TiO_2 global minimum candidate structures with the number of TiO_2 units in a cluster predicted by G_oW_o, qs*GW*, EA/IP-EOM-CCSD, ΔB3LYP, and KS-B3LYP using the def2-SVPD (SVD) and def2-TZVPP (TZ) basis sets. ΔPBE results can be found in Figure S2 in the Supporting Information.

$(TiO_2)_2$ dimer clusters, and the $(TiO_2)_3$ global minimum candidate cluster, as obtained with EA/IP-EOM-CCSD, ΔCCSD, ΔCCSD(T), and ΔCCSDT. The clusters seem to be dividable into two distinct sets: clusters for which EA/IP-EOM-CCSD and ΔCC methods predict similar values (i.e., the TiO_2 molecule and the $(TiO_2)_2$ trans cluster and $(TiO_2)_3$ global minimum candidate structure) and clusters for which EA/IP-EOM-CCSD and ΔCC methods give significantly different results for the IP (i.e., the $(TiO_2)_2$ cis and club clusters). The latter clusters are cases where the coupled-cluster calculation on the cation has large T1 amplitudes (e.g., 0.43 and 0.21 for the cis and club clusters, respectively, with CCSD/aug-cc-pVTZ). The large amplitudes suggest a significant multiconfigurational character of these cationic states and in turn that the $N - 1$ electron ROHF wave function might not be the best choice for a reference state. This in turn also might mean an unbalanced description of triples in CCSD(T) on this state. Since in EA/IP-EOM-CCSD the N electron RHF wave function of the neutral cluster is used instead as reference, such problems are circumvented and in such cases EA/IP-EOM-CCSD should yield more balanced results. The latter assessment is supported by the fact that the EA/IP-EOM-CCSD results show the same trends as G_0W_0 and qs*GW*, while the ΔCCSD and ΔCCSD(T) results display a completely different trend. For the other clusters there are some minor differences, especially with respect to ΔCCSD(T), probably related to the absence of a description of triples in EA/IP-EOM-CCSD. The difference between def2-TZVPP and aug-cc-pVTZ results, and thus the effect of adding diffuse functions, finally appears to be again small.

DOI: 10.1021/acs.jctc.7b00538
J. Chem. Theory Comput. 2017, 13, 3814−3828

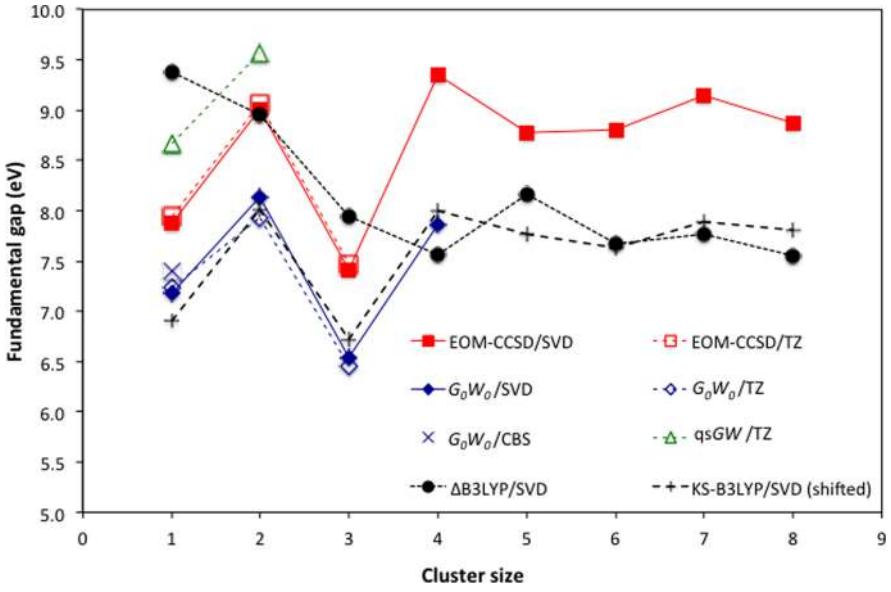

Figure 7. Trend in the fundamental gap of the TiO_2 global minimum candidate structures with the number of TiO_2 units in a cluster predicted by G_oW_o, qsGW, EA/IP-EOM-CCSD, ΔB3LYP, and KS-B3LYP using the def2-SVPD (SVD) and def2-TZVPP (TZ) basis sets. For the TiO_2 molecule the G_0W_0 result extrapolated to the complete basis-set limit (CBS) is also included. KS-B3LYP fundamental gap values are shifted upward by 3 eV. Unshifted KS-B3LYP and ΔPBE results can be found in Figure S3 in the Supporting Information.

Trends in Potentials and Fundamental Gap Values with Nanocluster Size for the Global Minimum Candidate Structures. Next, we study the evolution of −IP, −EA, and the fundamental gap with nanocluster size for the global minimum candidate structures. Figures 5−7 show the evolution of the predicted −IP, −EA, and fundamental gap values with nanocluster size for the different method combinations. As can be seen from Figures 5−7, as well as Tables 2, 3, and S2, G_0W_0, qsGW, and EA/IP-EOM-CCSD predict very similar trends for −IP and −EA with cluster size and between the different cluster isomers of $(TiO_2)_2$, irrespective of the basis set used. The three many-body methods differ, however, in the predicted absolute values. qsGW consistently predicts the deepest −IP values and G_0W_0 the most shallow. For −EA the differences are, just as in the case of the effect of basis-set size, smaller in absolute terms but larger in relative terms. ΔB3LYP predicts −IP and −EA values in roughly the same energy range as the three many-body methods, but displays a different ordering in the case of −IP, as well as suffers from the basis-set issues discussed above. KS-B3LYP predicts the same ordering as the many-body methods but yields much shallower −IP values and much deeper −EA values. While we only consider vertical potentials at this stage and hence cannot directly compare to experimental data, we expect similar observations to hold for adiabatic potentials, something that we consider in more detail below.

Any issue with describing −IP and −EA inherently carries over to the description of the fundamental gap by any given method combination. Not surprisingly thus all three many-body methods predict a similar nonmonotonic evolution of the fundamental gap with cluster size, where, in line with the error cancelation for the fundamental gap discussed above, the effect of the basis-set size on the calculated gap is very small for both G_0W_0 and EA/IP-EOM-CCSD. qsGW consistently predicts the largest fundamental gap values while G_0W_0 predicts the smallest with EA-IP-EOM-CCSD fundamental gap values lying between those of the two GW approaches. ΔB3LYP predicts fundamental gap values in the same energy range as the many-body methods but with a distinctly different pattern of maxima and minima in the fundamental gap for the smaller clusters, primarily due to its inability to reproduce the many-body method trend for −IP, discussed above. KS-B3LYP (see Figure S3 in the Supporting Information) in contrast predicts the same correct trend in the fundamental gap as the many-body methods but, not surprisingly, absolute gap values that are approximately twice as small as those found by G_0W_0 and EA/IP-EOM-CCSD.

Concentrating on the EA/IP-EOM-CCSD/def2-SVPD results, it appears that the clusters' IP values generally decrease with increasing cluster size for the global minima candidate structures. A similar trend can be seen for the −EA values, but here the undulations superimposed on this apparent trend are relatively larger than for the −IP values such that, over the size range considered, the $(TiO_2)_3$ minimum candidate structure has the deepest −EA value. The fundamental gap, finally, first appears to increase and then becomes more or less constant with increasing cluster size, but shows a dramatic dip for $(TiO_2)_3$. This deep dip in the fundamental gap for $(TiO_2)_3$ appears to be the direct result of the cluster's relatively deep −EA value, which might be linked to the fact that the structure has an exposed three-coordinated titanium atom with a low onsite electrostatic potential; see below.

Considering the additional low-energy isomers studied for $(TiO)_2$ and $(TiO)_3$, it is clear, see Table S2, that higher energy structures can have either more or less negative −IP values than the corresponding global minimum candidate structure, either more or less negative −EA values, and either larger or smaller fundamental gap values. It thus stands to reason that the trends in −EA, −IP, and the fundamental gap shown in Figures 5−7 are more likely the result of an underlying trend with cluster size in the types of structures that lie low in energy and the types of structural motives present in them than a direct effect of the cluster size per se.

Multiconfigurational Effects in EOM-CCSD. To illustrate the electronic structure of the $N \pm 1$ electronic states corresponding to lowest IPs and EAs, in Table 4 we display

DOI: 10.1021/acs.jctc.7b00538
J. Chem. Theory Comput. 2017, 13, 3814−3828

Table 4. Leading IP and EA EOM-CCSD Excitations Corresponding to the Lowest Values of the Ionization Potential and Electron Affinity of $(TiO_2)_n$ Cluster for $n = 1-5$[a]

	−VIP values	IP leading excitations	−VEA value	EA leading excitations
1	1^2B_1 (−9.53)	$r^H = -0.95$	1^2A_1 (−1.65)	$r_L = 0.98$
2 trans	1^2A (−10.36)	$r^H = -0.93$	1^2A (−1.35)	$r_L = 0.95$
				$r_{L+5} = 0.15$
				$r_{L+10} = 0.12$
2 cis	1^2B^1 (−9.98)	$r^H = -0.94$	1^2A_1 (−1.65)	$r_L = 0.96$
		$r^{H-7} = -0.14$		$r_{L+6} = 0.18$
2 club	$1^2A''$ (−9.60)	$r^H = -0.95$	$1^2A'$ (−1.93)	$r_L = 0.95$
				$r_{L+3} = 0.17$
3	$1^2A'$ (−10.07)	$r^H = -0.93$	$1^2A'$ (−2.66)	$r_L = 0.94$
		$r^{H-8} = 0.12$		$r_{L+3} = -0.19$
4	1^2A_2 (−10.89)	$r^H = -0.87$	1^2A_1 (−1.54)	$r_{L+3} = 0.89$
		$r^{H-8} = -0.37$		$r_{L+5} = -0.29$
5	$1^2A''$ (−10.76)	$r^H = -0.63$	$1^2A'$ (−1.99)	$r_L = 0.86$
		$r^{H-2} = -0.64$		$r_{L+1} = -0.15$
		$r^{H-4} = -0.13$		$r_{L+5} = -0.28$
		$r^{H-7} = 0.19$		$r_{L+7} = -0.20$
		$r^{H-12} = 0.15$		

[a]All values have been obtained with the def2-SVPD basis set, and the NWChem normalization convention is assumed in calculated values of r^i and r_a amplitudes.

Table 5. Vertical −IP and −EA Values of Orthotitanic Acid $Ti(OH)_4$ (1-OH) and the Hydroxylated $(TiO_2)_2(H_2O)_2$ (2-OH) Clusters Calculated by the Different Approaches Using Either def-SVPD or def2-TZVPP (def2-TZVPP Results in Bold) Basis Sets[a]

	KS-B3LYP		ΔB3LYP		G_0W_0		qsGW		EOM-CCSD	
	−VIP	−VEA	−VIP	−VEA	−VIP	−VEA	−VIP	−VEA	−VIP	−VEA
1-OH	**−8.59**	**−1.48**	**−10.86**	**0.78**	**−10.25**	**0.55**	**−11.75**	**0.99**	**−11.57**	**0.65**
1-OH	−8.72	−1.71	−10.97	0.53	−9.95	0.83			−11.51	0.66
2-OH	−8.47	−2.49	−10.76	−0.31	−9.38	−0.21			−10.84	−0.32

[a]G_0W_0 and qsGW calculations started from DFT calculation with the B3LYP XC functional. All values are in electronvolts.

the leading excitations defining the EA/IP-EOM-CCSD IP and EA $R(k)$ operators for $(TiO_2)_{1-5}$ (Table S3 in the Supporting Information shows the same information for larger clusters). For IPs the r^H $(=r^{\bar{H}})$, r^{H-1} $(=r^{\overline{H-1}})$, and so on singly excited amplitudes correspond to the removal of an α (β) electron from HOMO and HOMO−1 orbitals, respectively. A similar convention has been assumed to characterize the EA states. It is interesting to notice that, for the TiO_2 molecule, where the IP (cationic) and EA (anionic) electronic states are dominated by determinants obtained from the N electron HF Slater determinant by removing/adding one electron from/to HOMO/LUMO orbitals, for larger $(TiO_2)_n$ clusters the structure of these states becomes increasingly more multiconfigurational. This departure from the single determinantal picture implied by Koopmans theorem is best illustrated by the example of the $(TiO_2)_5$ cluster where five orbital (or 10 spin−orbital) excitations contribute to the $N-1$ electron coupled-cluster wave function with weight factors greater than 0.1. Something similar was previously observed by us for the excited states of small TiO_2 clusters.[40]

Hydroxylation. In the presence of water, the surface of TiO_2 particles will be (partly) hydroxylated. Water molecules will react with undercoordinated titanium and oxygen atoms on the surface to form surface hydroxyls. We studied the effect of hydroxylation by comparing results for the hydroxylated monomer $(TiO_2)(H_2O)_2$, orthotitanic acid $(Ti(OH)_4)$, with those for (TiO_2), as well as those of the dimer global minimum candidate structure (the trans dimer cluster) and its hydroxylated counterpart. As can be seen from a comparison of Tables 2, 3, S2, and 5, all methods predict that for both clusters' hydroxylation shifts the IP and −EA values downward and upward, respectively, and increases the size of the fundamental gap. However, the methods disagree on the exact nature and magnitude of the changes. Specifically, ΔB3LYP predicts only a small change in −IP and a large change in −EA for both clusters, while all other methods, including the use of the KS orbital energies, yield significant changes in both −IP and −EA for the monomer, and in the case of G_0W_0 and EA-IP-EOM-CCSD significant changes in −IP and small changes in −EA for the dimer. Just as for the nonhydroxylated clusters the KS-B3LYP results again lie far away from the GW and CC results, while for ΔB3LYP the match with GW and CC results improves.

Exciton Binding Energy. When making the assumption that for all clusters in our study the lowest excited state is bright, i.e., not symmetry forbidden, we can then use (EA/IP)-EOM-CCSD to calculate their fundamental and optical gaps in a consistent approach and extract information about the exciton binding energy in these clusters. The result of such a comparison is shown in Table 6, which shows, as expected, that the fundamental gap is always predicted to be considerably larger than the optical gap. The exciton binding energy appears to decrease with increasing cluster size but not in a monotonous fashion.

The hydroxylated clusters, while having fundamental and optical gaps that are much larger than their nonhydroxylated

DOI: 10.1021/acs.jctc.7b00538
J. Chem. Theory Comput. 2017, 13, 3814−3828

Table 6. Values of the Fundamental (ΔE_g) and Optical (ΔE_o) Gaps and Exciton Binding Energy (EBE) for a Range of (Hydroxlated) TiO_2 Nanoclusters Calculated Using (EA/IP)-EOM-CCSD and the def2-SVPD (SVD) and def2-TZVPP (TZ) Basis Sets[a]

	ΔE_f		ΔE_0		EBE	
	SVD	TZ	SVD	TZ	SVD	TZ
1	7.88	7.94	2.48	2.51	5.40	5.43
2 trans	9.01	9.07	3.84	3.71	5.17	5.18
2 cis	8.33	8.39	3.45	3.49	4.88	4.90
2 club	7.67	7.79	2.63	2.78	5.03	5.01
3	7.41	7.47	3.99	4.09	3.42	3.38
4	9.35		4.47		4.88	
5	8.77		4.14		4.63	
1-OH	12.17	12.22	6.40	6.51	5.77	5.71
2-OH	10.52		5.18		5.34	

[a]As discussed in the Introduction, we approximate the optical gap by the lowest vertical singlet excitation energy. All values are in electronvolts. 1-OH stands for the $Ti(OH)_4$ molecule and 2-OH for the hydroxylated $(TiO_2)_2(H_2O)_2$ cluster.

counterparts, have exciton binding energies that are comparable to the other clusters. While hydroxylation thus opens up the fundamental and optical gaps, it does not appear to significantly influence the screening of the excited electron−hole interaction and thus the exciton binding energy.

The exciton binding energy values of both the bare and hydrated clusters, are approximately 3 orders of magnitude larger than that measured for the bulk.[102] Similar dramatic increases in the exciton binding energy, when going from the bulk to nanoscale, have been predicted[103−106] and experimentally observed[107] for other systems and are probably due to the effect of a combination of increased overlap between hole and electron and reduced dielectric screening of the interaction between them in such small systems.

Finally, Table S4 in the Supporting Information provides estimates from ΔCCSD of the excitation energy toward the lowest triplet exciton for selected clusters. As expected, and in line with Hund's rule, comparing these ΔCCSD estimates with the EOM-CCSD optical gap values in Table 6 shows that the lowest energy triplet exciton generally lies lower in energy than the lowest singlet exciton, on the order of hundreds of millielectronvolts and that hence the lowest energy triplet exciton typically is more strongly bound than its singlet counterpart.

Adiabatic Potentials. We approximate adiabatic potentials and vertical potentials for the relaxed anion and cation, respectively, by optimizing the anion and cation geometries, respectively, using a setup similar to that of the ground state geometries (i.e., B3LYP/def2-TZVP) and performing single-point ΔB3LYP/def2-TZVPP, G_0W_0/def2-TZVPP, and EA/IP-EOM-CCSD/def2-TZVPP calculations on the relaxed anion and cation geometries.Tables 7 and 8 below give vertical −EA values for the anions and vertical −IP values for the cations, as well as adiabatic −EA and −IP values for the TiO_2 molecule and the $(TiO_2)_2$ and $(TiO_2)_3$ clusters. For $(TiO_2)_2$ we consider the three different possible isomers, which is critical when comparing to experiment; see below. In all cases, we have employed no symmetry constraints and verified that the relaxed anion and cation geometries correspond to proper minima and where required have distorted the geometries along imaginary modes and reoptimized the geometries until minima were

Table 7. Values of the Vertical −EA and −IP for the Anionic and Cationic Versions, Respectively, of the TiO_2 Molecule, the Different $(TiO_2)_2$ Clusters, and the $(TiO_2)_3$ Tentative Global Minimum Candidate Structure, As Predicted by ΔB3LYP, G_0W_0, and EA/IP-EOM-CCSD in Combination with a def2-TZVPP Basis Set[a]

	expt	ΔB3LYP		G_0W_0		EA/I-P-EOM-CCSD	
	−VEA anion	−VEA anion	−VIP cation	−VEA anion	−VIP cation	−VEA anion	−VIP cation
1	−1.59	−1.57	−9.17	−1.66	−8.25	−1.72	−9.03
2 trans		−2.17	−8.55	−2.26	−7.71	−1.95	−8.74
2 cis		−2.40	−8.40	−2.50	−7.60	−2.23	−8.92
2 club	−2.27	−2.31	−8.55	−2.33	−7.71	−2.35	−8.74
3	−3.15	−3.38	−8.19	−3.53	−7.31	−3.40	−8.48

[a]ΔB3LYP/def2-TZVP results can be found in Table S4 of the Supporting Information. Corresponding literature G_0W_0 −VEA values for the $(TiO_2)_2$ and $(TiO_2)_3$ clusters from Marom and co-workers are −1.95, −2.27, −2.26, and −3.28 eV, respectively. Experimental values taken from ref 18. All values are in electronvolts.

Table 8. Values of the Adiabatic −EA and −IP (−AEA and −AIP) of the TiO_2 Molecule, the Different $(TiO_2)_2$ Clusters, and the $(TiO_2)_3$ Tentative Global Minimum Candidate Structure, As Predicted by ΔB3LYP and EA/IP-EOM-CCSD in Combination with a def2-TZVPP Basis Set[a]

	expt	ΔB3LYP		EA/IP-EOM-CCSD	
	−AEA	−AEA	−AIP	−AEA	−AIP
1	−1.59	−1.50	−9.54	−1.46	−9.46
2 trans		−1.71	−9.51	−1.58	−9.84
2 cis		−1.95	−9.37	−1.87	−10.03
2 club	−2.06	−2.04	−8.80	−1.98	−9.14
3	−2.78	−2.95	−9.24	−2.87	−9.65

[a]ΔB3LYP/def2-TZVP, ΔCCSD/def2-TZVPP, and ΔCCSD(T)/def2-TZVPP results can be found in Tables S5 and S6 of the Supporting Information. Corresponding literature ΔCCSD(T) −AEA values from Dixon and co-workers for the TiO_2 molecule and the $(TiO_2)_2$ and $(TiO_2)_3$ clusters are −1.66, −1.64, −1.95, −1.98, and −2.88 eV, respectively.[58] Experimental values are taken from ref 18. All values are in electronvolts.

obtained. The cationic version of the club isomer of $(TiO_2)_2$ spontaneously interconverts into the trans isomer during optimization. All other clusters retain their approximate topology after optimization as anion or cation.

First, we compare our predicted −EA values to previous computational results from the literature. The G_0W_0 vertical −EA values for the different $(TiO_2)_2$ isomers in Table 7 are similar to the corresponding G_0W_0 values by Marom et al.,[38] even if the match is worse than for the neutral cluster geometries. The EA/IP-EOM-CCSD adiabatic −EA values in Table 8 can be compared with the recent ΔCCSD(T) results of Dixon and co-workers.[58] Doing so we find an identical energy ordering of the predicted adiabatic −EA values for both approaches and a reasonable match between the explicit values (see the Supporting Information for a comparison of Dixon's and our ΔCCSD(T) results). In both cases some of the differences could be attributable to a different description of the anion potential energy surface and hence slightly different anion minimum energy geometries rather than the method used to calculate the electron affinity.

DOI: 10.1021/acs.jctc.7b00538
J. Chem. Theory Comput. 2017, 13, 3814−3828

The G_0W_0 and EA/IP-EOM-CCSD predictions of the vertical −EA and −IP for the optimized anionic and cationic clusters geometries in Table 7 display, as expected from the experience with both methods for neutral cluster geometries, similar trends, bar a minor disagreement about the relative −EA of the cis and club isomers. The observation that IP-EOM-CCSD consistently predicts deeper IP values than G_0W_0 is also reproduced for the optimized cationic cluster geometries. More interestingly, ΔB3LYP appears to perform much better for the optimized anionic and cationic clusters geometries than for their neutral counterparts.

Comparison with vertical and adiabatic −EA values measured for size-selected anionic clusters by Wang's group[17,18] using a combination of mass spectrometry and photoelectron spectroscopy requires, in the case of the larger clusters, external input regarding which of the possible isomers is present. We follow here the assumption by Marom and co-workers[38] that the experimental cluster generation method employed preferentially generates the isomer with the most positive vertical EA (most negative vertical −EA) value for the corresponding neutral cluster. Based on both their and our results (see Tables 2 and 3) the relevant structure in the case of $(TiO_2)_2$ is then the club isomer, while for $(TiO_2)_3$ they predict that the neutral global minimum candidate structure has the most positive vertical EA. Focusing on these cluster structures that are most likely to accept an electron, we find a good fit between the experimentally measured vertical and adiabatic −EA values and the predictions by ΔB3LYP, G_0W_0, and EA/IP-EOM-CCSD.

Not surprisingly, relaxation results in deeper, i.e., more negative, vertical −EA values and more shallow, i.e., less negative, vertical −IP values. More interesting, G_0W_0 and EA/IP-EOM-CCSD predict very similar changes when comparing vertical potentials for the neutral and relaxed anion/cation structures. Also both for −EA and −IP the changes are roughly 2−8 times as large for the $(TiO_2)_2$ isomers than for the TiO_2 molecule, while the change in −IP values is 2−5 times as large as that in −EA. Holes thus appear to be considerably more strongly trapped than electrons, while it seems that larger clusters allow for more relaxation. The differences between the vertical −EA and −IP values of the neutral clusters and their adiabatic counterparts is considerably smaller and for selected cases even positive (−EA, TiO_2 molecule) or negative (−IP, cis isomer of $(TiO_2)_2$), respectively. It thus appears that any stabilization of the anionic/cationic state upon relaxation is largely compensated for by a destabilization of the neutral state. ΔB3LYP calculations yield a similar picture other than that holes are predicted to trap much stronger. As a result ΔB3LYP predicts, in contrast to ΔG_0W_0 and IP-EOM-CCSD, adiabatic −IP values that are considerably shallower than their vertical counterparts for neutral structures.

Microscopic Picture. Considering the leading excitation contributions to the EA/IP-EOM-CCSD vertical −IP and −EA values in Table 4 for the different clusters and their HF orbitals (see Figures S4−S6 in the Supporting Information), it is clear that in all cases the anion involves the localization of an excess electron on the most exposed titanium atom with the smallest number of coordinating oxygen atoms. In some cases, multiple titanium atoms are involved, e.g., in the $(TiO_2)_2$ trans and $(TiO_2)_4$ global minimum candidate structures, but generally these atoms are symmetry equivalent. In all cases the relevant titanium atoms are those with the least negative onsite electrostatic potential (calculated using the formal ionic charges, equivalent of the Madelung potential in crystalline solids) suggesting a possible correlation between −VEA and cluster electrostatics. Such a localization makes sense, as simple electrostatics would suggest that the energetic penalty of localizing an excess electron on an atom should decrease when the onsite electostatic potential becomes less negative. Finally, as previously observed by Marom and co-workers,[38,55] the environment of these exposed titanium atoms, on which the excess electron localizes, can be reminiscent of that of Ti^{3+} sites on TiO_2 surfaces. However, we should stress that all atoms in all clusters studied here have similar charges and there is no evidence for charge transfer. Indeed this is where semi-ionic materials such as TiO_2[108] differ from a semicovalent materials such as SiO_2, where there can be charge transfer in the ground state of nanoclusters, e.g., so-called valence alternation pairs.[109]

The case of the cations, and hence the −IP values of the clusters, is more complicated. First, the relevant orbitals (e.g., HOMO) are often very delocalized, involving multiple distinct types of oxygen atoms: for example, both the one- and two-coordinated oxygen atoms in the $(TiO_2)_2$ trans global minimum candidate structure; second, while a similar electrostatic argument can be made as for the anion that the hole should localize on the oxygen atom with the least positive onsite electrostatic potential, typically, a terminal 1-coordinated oxygen atom. There are also cases, e.g., the $(TiO_2)_2$ club structure, where the hole localizes on other oxygen atoms instead (the three two-coordinated oxygen atoms in the case of the club structure). The link between the −VIP value and the onsite electrostatic potential appears thus weaker than for −VEA. Visual inspection suggests that an additional contributing factor might be the number of atoms over which relevant orbitals are delocalized. The especially strong multiconfigurational character of the IP for the $(TiO_2)_5$ global minimum candidate structure, discussed above, appears linked to the existence of two near degenerate orbitals centered around the one-coordinated oxygen atoms on opposite sides of the cluster, which are not symmetry equivalent.

The effect of hydroxylation on −IP, −EA, and the fundamental gap can at least in part be explained by changes in the electrostatic environment of atoms. Hydroxylation increases the coordination number of undercoordinated atoms and increases the onsite electrostatic potential for such atoms and destabilizes the localization of electrons or holes on them. As previously observed in terms of the optical gap of TiO_2 nanoclusters,[44,45] hydroxylation averages out the electronic structure of clusters by "normalizing" the electrostatic environment of atoms.

It is tempting to blame the apparent failure of ΔB3LYP to predict exactly how −IP and −EA values vary between different bare TiO_2 clusters on the multiconfigurational nature of the cationic and anionic states of the clusters discussed above. The problem, however, with this explanation is that the use of the B3LYP KS orbital energies results in the successful recovery of the trends found for the many-body methods. Likely, the problem is more subtle and related, at least in part, to the localization of the hole and excess electron in the cation/anion and how this is described by DFT. This would explain why ΔB3LYP appears to perform better for relaxed anionic and cationic structures, in which by necessity the excess electron/hole is unambiguously more localized. It also would be in line with the observation, discussed above, of the SCF for the cations of selected clusters converging to solutions with different spin distributions when changing the basis set and this resulting in substantially different predictions for −IP.

DOI: 10.1021/acs.jctc.7b00538
J. Chem. Theory Comput. 2017, 13, 3814−3828

Finally, the notion that a good description of (de)localization is important is also supported by the fact that ΔDFT calculations using the PBE XC functional, which tends to give a more delocalized description, predict a different trend than that obtained with ΔB3LYP (see Figures S1−S3 in the Supporting Information).

CONCLUSIONS

We studied the ionization potentials, electron affinities, fundamental gaps, and exciton binding energies of small TiO_2 nanoclusters using a range of methods. We demonstrate that all many-body methods considered predict similar trends, but that G_0W_0 appears rather sensitive to basis-set size. Moreover, we find that the difference between qsGW and G_0W_0 predictions is generally larger than those between either of the GW approaches and EA/IP-EOM-CCSD. Specifically, in the case of −IP values, G_0W_0 predicts the shallowest vertical potentials and qsGW the deepest, with the vertical −IP predicted by the EA/IP-EOM-CCSD method lying between the two but closer to the latter. Similarly, G_0W_0 predicts the smallest fundamental gap values, qsGW the largest, and EA/IP-EOM-CCSD values roughly intermediate between both Green's function methods. For the vertical −EA values, the absolute difference in prediction between the three methods is smaller though not necessarily in relative terms. The B3LYP highest occupied and lowest unoccupied orbitals follow the same trends as those predicted by the many-body methods for −IP and −EA but are generally far too shallow and deep, respectively, in absolute terms. The total energy ΔB3LYP method, in contrast, yields values in the correct energy window but predicts different trends than the many-body methods in all electronic properties with cluster size. Assuming that the qsGW and IP/EA-EOM-CCSD methods are inherently the most accurate approaches among those studied, our results suggest that while ΔB3LYP allows one to predict the correct orders of magnitude of vertical −IP and −EA for bare TiO_2 clusters, the prediction of accurate trends in vertical −IP and −EA values appears to require a more advanced approach than ΔB3LYP and probably by extension ΔDFT in general. Conversely, G_0W_0, at least when using B3LYP orbitals as a starting point, allows one to accurately predict trends in −IP and −EA, but appears less reliable in terms of absolute values, especially in the case of −IP, although we cannot rule out this being in part due to different convergence rates with respect to basis-set size. Calculations of vertical potential values for the relaxed cation/anion cluster geometries, as well as adiabatic potentials, generally display the same performance as the vertical potentials for the neutral cluster, other than an improved performance of ΔB3LYP, and in the case of −EA a good fit to experiment.

All electronic properties considered in this work are shown to vary nonmonotonically with cluster size while hydroxylation of undercoordinated atoms is demonstrated to be linked to an opening up of the fundamental gap and thus −IP moving deeper and −EA slightly shallower. We suggest that the change with cluster size, as well as upon hydroxylation, can be understood, at least in part, in terms of the on-site electrostatic potential and the number of atoms states are delocalized over. The exciton binding energy in these small clusters appears to decrease with increasing cluster size but again in a nonmonotonic fashion, while hydroxylation, in contrast, results in no real change in the exciton binding energy relative to the unhydroxylated bare clusters. Structural relaxation after removal/addition of an electron, i.e., trapping, is found to be consistently stronger for holes than electrons. The net effect on the predicted adiabatic potentials is, however, found to be relatively small because the stabilization of the cationic/anionic state is largely compensated for by a destabilization of the neutral state.

ASSOCIATED CONTENT

Supporting Information

The Supporting Information is available free of charge on the ACS Publications website at DOI: 10.1021/acs.jctc.7b00538.

Tabulated −IP and −EA values for the TiO_2 molecule predicted with a range of basis sets, def2-SVPD −IP and −EA values for TiO_2 to $(TiO_2)_4$, leading IP/EA-EOM-CCSD excitations, PBE XC-functional results and plots of relevant orbitals (PDF)

xyz coordinates of B3LYP/def2-TZVP optimized anion and cation geometries of TiO_2, $(TiO_2)_2$, and $(TiO_2)_3$, and calculated atomic on-site electrostatic potentials for all neutral clusters (ZIP)

AUTHOR INFORMATION

Corresponding Authors

*(M.J.v.S.) E-mail: michiel.vansetten@uclouvain.be.
*(K.K.) E-mail: karol.kowalski@pnnl.gov.
*(M.A.Z.) E-mail: m.zwijnenburg@ucl.ac.uk.

ORCID

Karol Kowalski: 0000-0001-6357-785X
Martijn A. Zwijnenburg: 0000-0001-5291-2130

Funding

M.A.Z. acknowledges the U.K. Engineering and Physical Sciences Research Council (EPSRC) for a Career Acceleration Fellowship (Grant EP/I004424/1). U.K.'s HPC Materials Chemistry Consortium is funded by EPSRC (Grant EP/L000202/1). The Pacific Northwest National Laboratory is operated for the US Department of Energy by the Battelle Memorial Institute under Contract No. DE-AC06.76RLO-1830. The computational work conducted by W.A.S. is supported by the U.S. Department of Energy under EPSCoR Grant No. DE-SC0012432 with additional support from the Louisiana Board of Regents.

Notes

The authors declare no competing financial interest.

ACKNOWLEDGMENTS

We kindly acknowledge Prof. S.T. Bromley, Prof. D. Dixon, Prof. F. Evers, Dr. N. Govind, Mr. R. Hilali, Prof. G.-M. Rignanese, and Dr. S. M. Woodley for stimulating discussions. M.A.Z. thanks Dr. K. E. Jelfs and Ms. R. A. Zwijnenburg for making the timely completion of this manuscript possible. Computational time on ARCHER, the U.K.'s national high-performance computing service (via our membership with the U.K.'s HPC Materials Chemistry Consortium) and at the HC3 cluster at the Karlsruhe Institute of Technology (KIT) Steinbuch Center for Computing (SCC) is gratefully acknowledged. Part of the work has been performed using EMSL, a national scientific user facility sponsored by the Department of Energy's Office of Biological and Environmental Research and located at Pacific Northwest National Laboratory.

DOI: 10.1021/acs.jctc.7b00538
J. Chem. Theory Comput. 2017, 13, 3814−3828

REFERENCES

(1) Bhatkhande, D. S.; Pangarkar, V. G.; Beenackers, A. A. C. M. Photocatalytic degradation for environmental applications - A review. *J. Chem. Technol. Biotechnol.* **2002**, *77*, 102−116.

(2) Lydakis-Simantiris, N.; Riga, D.; Katsivela, E.; Mantzavinos, D.; Xekoukoulotakis, N. P. Disinfection of spring water and secondary treated municipal wastewater by TiO_2 photocatalysis. *Desalination* **2010**, *250*, 351−355.

(3) Wang, C.; Liu, H.; Qu, Y. TiO_2-based photocatalytic process for purification of polluted water: Bridging fundamentals to applications. *J. Nanomater.* **2013**, *2013*, 319637.

(4) Li, D.; Haneda, H.; Hishita, S.; Ohashi, N. Visible-Light-Driven N−F−Codoped TiO_2 Photocatalysts. 2. Optical Characterization, Photocatalysis, and Potential Application to Air Purification. *Chem. Mater.* **2005**, *17*, 2596−2602.

(5) Maeda, K. Direct splitting of pure water into hydrogen and oxygen using rutile titania powder as a photocatalyst. *Chem. Commun.* **2013**, *49*, 8404−8406.

(6) Maeda, K. Photocatalytic properties of rutile TiO_2 powder for overall water splitting. *Catal. Sci. Technol.* **2014**, *4*, 1949−1953.

(7) Maeda, K.; Murakami, N.; Ohno, T. Dependence of Activity of Rutile Titanium(IV) Oxide Powder for Photocatalytic Overall Water Splitting on Structural Properties. *J. Phys. Chem. C* **2014**, *118*, 9093−9100.

(8) Amano, F.; Nakata, M.; Ishinaga, E. Photocatalytic Activity of Rutile Titania for Hydrogen Evolution. *Chem. Lett.* **2014**, *43*, 509−511.

(9) Sato, S.; White, J. M. Photodecomposition of water over Pt/TiO_2 catalysts. *Chem. Phys. Lett.* **1980**, *72*, 83−86.

(10) Tang, J.; Durrant, J. R.; Klug, D. R. Mechanism of photocatalytic water splitting in TiO_2. Reaction of water with photoholes, importance of charge carrier dynamics, and evidence for four-hole chemistry. *J. Am. Chem. Soc.* **2008**, *130*, 13885−13891.

(11) Banno, H.; Kariya, B.; Isu, N.; Ogawa, M.; Miwa, S.; Sawada, K.; Tsuge, J.; Imaizumi, S.; Kato, H.; Tokutake, K.; Deguchi, S. Effect of TiO_2 Crystallite Diameter on Photocatalytic Water Splitting Rate. *Green Sustainable Chem.* **2014**, *4*, 87−94.

(12) Grätzel, M. Solar energy conversion by dye-sensitized photovoltaic cells. *Inorg. Chem.* **2005**, *44*, 6841−6851.

(13) Zhang, S.; Yang, X.; Numata, Y.; Han, L. Highly efficient dye-sensitized solar cells: progress and future challenges. *Energy Environ. Sci.* **2013**, *6*, 1443−1464.

(14) Takeuchi, M.; Sakamoto, K.; Martra, G.; Coluccia, S.; Anpo, M. Mechanism of photoinduced superhydrophilicity on the TiO_2 photocatalyst surface. *J. Phys. Chem. B* **2005**, *109*, 15422−15428.

(15) Ganesh, V. A.; Raut, H. K.; Nair, A. S.; Ramakrishna, S. A review on self-cleaning coatings. *J. Mater. Chem.* **2011**, *21*, 16304−16322.

(16) Parkin, I. P.; Palgrave, R. G. Self-cleaning coatings. *J. Mater. Chem.* **2005**, *15*, 1689−1695.

(17) Wu, H.; Wang, L. S. Electronic structure of titanium oxide clusters: TiO_y (y = 1−3) and $(TiO_2)_n$ (n = 1−4). *J. Chem. Phys.* **1997**, *107*, 8221−8228.

(18) Zhai, H. J.; Wang, L. S. Probing the electronic structure and band gap evolution of titanium oxide clusters $(TiO_2)_n^-$ (n = 1−10) using photoelectron spectroscopy. *J. Am. Chem. Soc.* **2007**, *129*, 3022−3026.

(19) Schneider, J.; Matsuoka, M.; Takeuchi, M.; Zhang, J.; Horiuchi, Y.; Anpo, M.; Bahnemann, D. W. Understanding TiO_2 Photocatalysis: Mechanisms and Materials. *Chem. Rev.* **2014**, *114*, 9919−9986.

(20) Qu, Z. W.; Kroes, G. J. Theoretical study of the electronic structure and stability of titanium dioxide clusters $(TiO_2)_n$ with n = 1−9. *J. Phys. Chem. B* **2006**, *110*, 8998−9007.

(21) Li, S.; Dixon, D. A. Molecular structures and energetics of the $(TiO_2)_n$ (n = 1 - 4) clusters and their anions. *J. Phys. Chem. A* **2008**, *112*, 6646−6666.

(22) Calatayud, M.; Maldonado, L.; Minot, C. Reactivity of $(TiO_2)_n$ Clusters (n = 1 - 10): Probing Gas-Phase Acidity and Basicity Properties. *J. Phys. Chem. C* **2008**, *112*, 16087−16095.

(23) Blagojevic, V.; Chen, Y.-R.; Steigerwald, M.; Brus, L.; Friesner, R. A. Quantum Chemical Investigation of Cluster Models for TiO_2 Nanoparticles with Water-Derived Ligand Passivation: Studies of Excess Electron States and Implications for Charge Transport in the Gratzel Cell. *J. Phys. Chem. C* **2009**, *113*, 19806−19811.

(24) Calatayud, M.; Minot, C. Is There a Nanosize for the Activity of TiO_2 Compounds? *J. Phys. Chem. C* **2009**, *113*, 12186−12194.

(25) Mowbray, D. J.; Martinez, J. I.; García Lastra, J. M.; Thygesen, K. S.; Jacobsen, K. W. Stability and Electronic Properties of TiO_2 Nanostructures With and Without B and N Doping. *J. Phys. Chem. C* **2009**, *113*, 12301−12308.

(26) Shevlin, S. A.; Woodley, S. M. Electronic and Optical Properties of Doped and Undoped $(TiO_2)_n$ Nanoparticles. *J. Phys. Chem. C* **2010**, *114*, 17333−17343.

(27) Taylor, D. J.; Paterson, M. J. Calculations of the low-lying excited states of the TiO_2 molecule. *J. Chem. Phys.* **2010**, *133*, 204302.

(28) Kang, W.; Hybertsen, M. S. Quasiparticle and optical properties of rutile and anatase TiO_2. *Phys. Rev. B: Condens. Matter Mater. Phys.* **2010**, *82*, 085203.

(29) Chiodo, L.; Garcia-Lastra, J. M.; Iacomino, A.; Ossicini, S.; Zhao, J.; Petek, H.; Rubio, A. Self-energy and excitonic effects in the electronic and optical properties of TiO_2 crystalline phases. *Phys. Rev. B: Condens. Matter Mater. Phys.* **2010**, *82*, 045207.

(30) Auvinen, S.; Alatalo, M.; Haario, H.; Jalava, J. P.; Lamminmäki, R. J. Size and shape dependence of the electronic and spectral properties in TiO_2 nanoparticles. *J. Phys. Chem. C* **2011**, *115*, 8484−8493.

(31) Chiodo, L.; Salazar, M.; Romero, A. H.; Laricchia, S.; Sala, F. D.; Rubio, A. Structure, electronic, and optical properties of TiO_2 atomic clusters: an ab initio study. *J. Chem. Phys.* **2011**, *135*, 244704.

(32) Wang, T. H.; Fang, Z.; Gist, N. W.; Li, S.; Dixon, D. A.; Gole, J. L. Computational study of the hydrolysis reactions of the ground and first excited triplet states of small TiO_2 nanoclusters. *J. Phys. Chem. C* **2011**, *115*, 9344−9360.

(33) Di Valentin, C.; Selloni, A. Bulk and Surface Polarons in Photoexcited Anatase TiO_2. *J. Phys. Chem. Lett.* **2011**, *2*, 2223−2228.

(34) Syzgantseva, O. A.; Gonzalez-Navarrete, P.; Calatayud, M.; Bromley, S.; Minot, C. Theoretical Investigation of the Hydrogenation of $(TiO_2)_n$ Clusters (n = 1 - 10). *J. Phys. Chem. C* **2011**, *115*, 15890−15899.

(35) Marom, N.; Moussa, J. E.; Ren, X.; Tkatchenko, A.; Chelikowsky, J. R. Electronic structure of dye-sensitized TiO_2 clusters from many-body perturbation theory. *Phys. Rev. B: Condens. Matter Mater. Phys.* **2011**, *84*, 245115.

(36) Govind, N.; Lopata, K.; Rousseau, R.; Andersen, A.; Kowalski, K. Visible Light Absorption of N-Doped TiO_2 Rutile Using (LR/RT)-TDDFT and Active Space EOMCCSD Calculations. *J. Phys. Chem. Lett.* **2011**, *2*, 2696−2701.

(37) Taylor, D. J.; Paterson, M. J. Vibronic coupling effects on the structure and spectroscopy of neutral and charged TiO_2 clusters. *Chem. Phys.* **2012**, *408*, 1−10.

(38) Marom, N.; Kim, M.; Chelikowsky, J. R. Structure selection based on high vertical electron affinity for TiO_2 clusters. *Phys. Rev. Lett.* **2012**, *108*, 106801.

(39) Zhang, J.; Hughes, T. F.; Steigerwald, M.; Brus, L.; Friesner, R. A. Realistic cluster modeling of electron transport and trapping in solvated TiO_2 nanoparticles. *J. Am. Chem. Soc.* **2012**, *134*, 12028−12042.

(40) Berardo, E.; Hu, H.-S.; Kowalski, K.; Zwijnenburg, A. M. Coupled cluster calculations on TiO_2 nanoclusters. *J. Chem. Phys.* **2013**, *139*, 064313.

(41) Scanlon, D. O.; Dunnill, C. W.; Buckeridge, J.; Shevlin, S. A.; Logsdail, A. J.; Woodley, S. M.; Catlow, C. R. A.; Powell, M. J.; Palgrave, R. G.; Parkin, I. P.; Watson, G. W.; Keal, T. W.; Sherwood, P.; Walsh, A.; Sokol, A. A. Band alignment of rutile and anatase TiO_2. *Nat. Mater.* **2013**, *12*, 798−801.

(42) Chen, M.; Dixon, D. A. Tree growth - Hybrid genetic algorithm for predicting the structure of small $(TiO_2)_n$, n = 2−13, nanoclusters. *J. Chem. Theory Comput.* **2013**, *9*, 3189−3200.

DOI: 10.1021/acs.jctc.7b00538
J. Chem. Theory Comput. 2017, 13, 3814−3828

(43) Fang, Z. T.; Dixon, D. A. Computational Study of H-2 and O-2 Production from Water Splitting by Small $(MO_2)_n$ Clusters (M = Ti, Zr, Hf). *J. Phys. Chem. A* **2013**, *117*, 3539−3555.
(44) Berardo, E.; Hu, H.-S.; Shevlin, S. A.; Woodley, S. M.; Kowalski, K.; Zwijnenburg, M. A. Modeling Excited States in TiO_2 Nanoparticles: On the Accuracy of a TD-DFT Based Description. *J. Chem. Theory Comput.* **2014**, *10*, 1189−1199.
(45) Berardo, E.; Hu, H.-S.; van Dam, H. J. J.; Shevlin, S. A.; Woodley, S. M.; Kowalski, K.; Zwijnenburg, M. A. Describing Excited State Relaxation and Localization in TiO_2 Nanoparticles Using TD-DFT. *J. Chem. Theory Comput.* **2014**, *10*, 5538−5548.
(46) Marom, N.; Korzdorfer, T.; Ren, X. G.; Tkatchenko, A.; Chelikowsky, J. R. Size Effects in the Interface Level Alignment of Dye-Sensitized TiO_2 Clusters. *J. Phys. Chem. Lett.* **2014**, *5*, 2395−2401.
(47) Kapilashrami, M.; Zhang, Y.; Liu, Y.-S.; Hagfeldt, A.; Guo, J. Probing the Optical Property and Electronic Structure of TiO_2 Nanomaterials for Renewable Energy Applications. *Chem. Rev.* **2014**, *114*, 9662−9707.
(48) Hung, L.; Baishya, K.; Öğüt, S. First-principles real-space study of electronic and optical excitations in rutile TiO_2 nanocrystals. *Phys. Rev. B: Condens. Matter Mater. Phys.* **2014**, *90*, 165424.
(49) Zhang, J.; Steigerwald, M.; Brus, L.; Friesner, R. A. Covalent O-H Bonds as Electron Traps in Proton-Rich Rutile TiO_2 Nanoparticles. *Nano Lett.* **2014**, *14*, 1785−1789.
(50) Spreafico, C.; VandeVondele, J. The nature of excess electrons in anatase and rutile from hybrid DFT and RPA. *Phys. Chem. Chem. Phys.* **2014**, *16*, 26144−26152.
(51) Nunzi, F.; Agrawal, S.; Selloni, A.; De Angelis, F. Structural and Electronic Properties of Photoexcited TiO_2 Nanoparticles from First Principles. *J. Chem. Theory Comput.* **2015**, *11*, 635−645.
(52) Kazaryan, A.; van Santen, R.; Baerends, E. J. Light-induced water splitting by titanium-tetrahydroxide: a computational study. *Phys. Chem. Chem. Phys.* **2015**, *17*, 20308−20321.
(53) Berardo, E.; Zwijnenburg, M. A. Modeling the Water Splitting Activity of a TiO_2 Rutile Nanoparticle. *J. Phys. Chem. C* **2015**, *119*, 13384−13393.
(54) Buckeridge, J.; Butler, K. T.; Catlow, C. R. A.; Logsdail, A. J.; Scanlon, D. O.; Shevlin, S. A.; Woodley, S. M.; Sokol, A. A.; Walsh, A. Polymorph Engineering of TiO_2: Demonstrating How Absolute Reference Potentials Are Determined by Local Coordination. *Chem. Mater.* **2015**, *27*, 3844−3851.
(55) Bhattacharya, S.; Sonin, B. H.; Jumonville, C. J.; Ghiringhelli, L. M.; Marom, N. Computational design of nanoclusters by property-based genetic algorithms: Tuning the electronic properties of $(TiO_2)_n$ clusters. *Phys. Rev. B: Condens. Matter Mater. Phys.* **2015**, *91*, 241115.
(56) Luppi, E.; Urdaneta, I.; Calatayud, M. Photoactivity of Molecule−TiO_2 Clusters with Time-Dependent Density-Functional Theory. *J. Phys. Chem. A* **2016**, *120*, 5115−5124.
(57) Cho, D.; Ko, K. C.; Lamiel-García, O.; Bromley, S. T.; Lee, J. Y.; Illas, F. Effect of Size and Structure on the Ground-State and Excited-State Electronic Structure of TiO_2 Nanoparticles. *J. Chem. Theory Comput.* **2016**, *12*, 3751−3763.
(58) Fang, Z. T.; Both, J.; Li, S. G.; Yue, S. W.; Apra, E.; Keceli, M.; Wagner, A. F.; Dixon, D. A. Benchmark Calculations of Energetic Properties of Groups 4 and 6 Transition Metal Oxide Nanoclusters Including Comparison to Density Functional Theory. *J. Chem. Theory Comput.* **2016**, *12*, 3689−3710.
(59) Muuronen, M.; Parker, S. M.; Berardo, E.; Le, A.; Zwijnenburg, M. A.; Furche, F. Mechanism of photocatalytic water oxidation on small TiO_2 nanoparticles. *Chem. Sci.* **2017**, *8*, 2179−2183.
(60) Bredas, J. L. Mind the gap! *Mater. Horiz.* **2014**, *1*, 17−19.
(61) Kohn, W. Nobel Lecture: Electronic structure of matter-wave functions and density functionals. *Rev. Mod. Phys.* **1999**, *71*, 1253−1266.
(62) Baerends, E. J.; Gritsenko, O. V.; van Meer, R. The Kohn-Sham gap, the fundamental gap and the optical gap: the physical meaning of occupied and virtual Kohn-Sham orbital energies. *Phys. Chem. Chem. Phys.* **2013**, *15*, 16408−16425.
(63) Gunnarsson, O.; Lundqvist, B. I. Exchange And Correlation In Atoms, Molecules, And Solids By Spin-Density Functional Formalism. *Phys. Rev. B* **1976**, *13*, 4274−4298.
(64) Jones, R. O.; Gunnarsson, O. The Density Functional Formalism, Its Applications And Prospects. *Rev. Mod. Phys.* **1989**, *61*, 689−746.
(65) Runge, E.; Gross, E. K. U. Density-Functional Theory For Time-Dependent Systems. *Phys. Rev. Lett.* **1984**, *52*, 997−1000.
(66) Hedin, L. On correlation effects in electron spectroscopies and the GW approximation. *J. Phys.: Condens. Matter* **1999**, *11*, R489.
(67) Hedin, L. New Method for Calculating the One-Particle Green's Function with Application to the Electron-Gas Problem. *Phys. Rev.* **1965**, *139*, A796.
(68) Hedin, L. Effect Of Electron Correlation On Band Structure Of Solids. *Arkiv. Fys.* **1965**, *30*, 231.
(69) Onida, G.; Reining, L.; Rubio, A. Electronic excitations: density-functional versus many-body Green's-function approaches. *Rev. Mod. Phys.* **2002**, *74*, 601−659.
(70) Bartlett, R. J.; Musiał, M. Coupled-cluster theory in quantum chemistry. *Rev. Mod. Phys.* **2007**, *79*, 291−352.
(71) Comeau, D. C.; Bartlett, R. J. The equation-of-motion coupled-cluster method. Applications to open- and closed-shell reference states. *Chem. Phys. Lett.* **1993**, *207*, 414−423.
(72) Stanton, J. F.; Bartlett, R. J. The equation of motion coupled-cluster method. A systematic biorthogonal approach to molecular excitation energies, transition probabilities, and excited state properties. *J. Chem. Phys.* **1993**, *98*, 7029−7039.
(73) Geertsen, J.; Rittby, M.; Bartlett, R. J. The equation-of-motion coupled-cluster method: Excitation energies of Be and CO. *Chem. Phys. Lett.* **1989**, *164*, 57−62.
(74) Faleev, S. V.; van Schilfgaarde, M.; Kotani, T. All-electron self-consistent GW approximation: Application to Si, MnO, and NiO. *Phys. Rev. Lett.* **2004**, *93*, 126406.
(75) van Schilfgaarde, M.; Kotani, T.; Faleev, S. Quasiparticle self-consistent GW theory. *Phys. Rev. Lett.* **2006**, *96*, 226402.
(76) Kaplan, F.; Harding, M. E.; Seiler, C.; Weigend, F.; Evers, F.; van Setten, M. J. Quasi-Particle Self-Consistent GW for Molecules. *J. Chem. Theory Comput.* **2016**, *12*, 2528−2541.
(77) van Setten, M. J.; Weigend, F.; Evers, F. The GW-Method for Quantum Chemistry Applications: Theory and Implementation. *J. Chem. Theory Comput.* **2013**, *9*, 232−246.
(78) Bhaskaran-Nair, K.; Kowalski, K.; Moreno, J.; Jarrell, M.; Shelton, W. A. Equation of motion coupled cluster methods for electron attachment and ionization potential in fullerenes C-60 and C-70. *J. Chem. Phys.* **2014**, *141*, 074304.
(79) Yu, W.; Freas, R. B. Formation and fragmentation of gas-phase titanium/oxygen cluster positive ions. *J. Am. Chem. Soc.* **1990**, *112*, 7126−7133.
(80) Guo, B. C.; Kerns, K. P.; Castleman, A. W. Studies of reactions of small titanium oxide cluster cations toward oxygen at thermal energies. *Int. J. Mass Spectrom. Ion Processes* **1992**, *117*, 129−144.
(81) Becke, A. D. Density-functional thermochemistry 0.3. The role of exact exchange. *J. Chem. Phys.* **1993**, *98*, 5648−5652.
(82) Stephens, P. J.; Devlin, F. J.; Chabalowski, C. F.; Frisch, M. J. Ab-Initio Calculation Of Vibrational Absorption And Circular-Dichroism Spectra Using Density-Functional Force-Fields. *J. Phys. Chem.* **1994**, *98*, 11623−11627.
(83) Nooijen, M.; Snijders, J. G. Coupled Cluster Approach To The Single-Particle Green-Function. *Int. J. Quantum Chem.* **1992**, *44*, 55−83.
(84) Nooijen, M.; Snijders, J. G. Coupled-Cluster Green-Function Method - Working Equations And Applications. *Int. J. Quantum Chem.* **1993**, *48*, 15−48.
(85) Nooijen, M.; Snijders, J. G. Diagrammatic Analysis And Application Of The Coupled-Cluster Response Approach To Ground-State Expectation Values. *Int. J. Quantum Chem.* **1993**, *47*, 3−47.
(86) Meissner, L.; Bartlett, R. J. Electron propagator theory with the ground state correlated by the coupled-cluster method. *Int. J. Quantum Chem.* **1993**, *48*, 67−80.

DOI: 10.1021/acs.jctc.7b00538
J. Chem. Theory Comput. 2017, 13, 3814−3828

(87) Nooijen, M.; Snijders, J. G. 2nd-Order Many-Body Perturbation Approximations To The Coupled-Cluster Greens-Function. *J. Chem. Phys.* **1995**, *102*, 1681−1688.
(88) Bhaskaran-Nair, K.; Kowalski, K.; Shelton, W. A. Coupled cluster Green function: Model involving single and double excitations. *J. Chem. Phys.* **2016**, *144*, 144101.
(89) Kowalski, K.; Bhaskaran-Nair, K.; Shelton, W. A. Coupled-cluster representation of Green function employing modified spectral resolutions of similarity transformed Hamiltonians. *J. Chem. Phys.* **2014**, *141*, 094102.
(90) Peng, B.; Kowalski, K. Coupled-cluster Green's function: Analysis of properties originating in the exponential parametrization of the ground-state wave function. *Phys. Rev. A: At., Mol., Opt. Phys.* **2016**, *94*, 062512.
(91) Kaplan, F.; Weigend, F.; Evers, F.; van Setten, M. J. Off-Diagonal Self-Energy Terms and Partially Self-Consistency in GW Calculations for Single Molecules: Efficient Implementation and Quantitative Effects on Ionization Potentials. *J. Chem. Theory Comput.* **2015**, *11*, 5152−5160.
(92) Hamad, S.; Catlow, C. R. A.; Woodley, S. M.; Lago, S.; Mejias, J. A. Structure and stability of small TiO_2 nanoparticles. *J. Phys. Chem. B* **2005**, *109*, 15741−15748.
(93) Weigend, F.; Haser, M.; Patzelt, H.; Ahlrichs, R. RI-MP2: optimized auxiliary basis sets and demonstration of efficiency. *Chem. Phys. Lett.* **1998**, *294*, 143−152.
(94) Weigend, F.; Ahlrichs, R. Balanced basis sets of split valence, triple zeta valence and quadruple zeta valence quality for H to Rn: Design and assessment of accuracy. *Phys. Chem. Chem. Phys.* **2005**, *7*, 3297−3305.
(95) Ahlrichs, R.; Bar, M.; Haser, M.; Horn, H.; Kolmel, C. Electronic-Structure Calculations On Workstation Computers - The Program System Turbomole. *Chem. Phys. Lett.* **1989**, *162*, 165−169.
(96) Furche, F.; Ahlrichs, R.; Haettig, C.; Klopper, W.; Sierka, M.; Weigend, F. Turbomole. *WIREs Comput. Mol. Sci.* **2014**, *4*, 91−100.
(97) Valiev, M.; Bylaska, E. J.; Govind, N.; Kowalski, K.; Straatsma, T. P.; Van Dam, H. J. J.; Wang, D.; Nieplocha, J.; Apra, E.; Windus, T. L.; de Jong, W. NWChem: A comprehensive and scalable open-source solution for large scale molecular simulations. *Comput. Phys. Commun.* **2010**, *181*, 1477−1489.
(98) Schafer, A.; Horn, H.; Ahlrichs, R. Fully Optimized Contracted Gaussian-Basis Sets For Atoms Li To Kr. *J. Chem. Phys.* **1992**, *97*, 2571−2577.
(99) Dunning, T. H. Gaussian-Basis Sets For Use In Correlated Molecular Calculations 0.1. The Atoms Boron Through Neon And Hydrogen. *J. Chem. Phys.* **1989**, *90*, 1007−1023.
(100) Balabanov, N. B.; Peterson, K. A. Systematically convergent basis sets for transition metals. I. All-electron correlation consistent basis sets for the 3d elements Sc-Zn. *J. Chem. Phys.* **2005**, *123*, 064107.
(101) van Setten, M. J.; Caruso, F.; Sharifzadeh, S.; Ren, X. G.; Scheffler, M.; Liu, F.; Lischner, J.; Lin, L.; Deslippe, J. R.; Louie, S. G.; Yang, C.; Weigend, F.; Neaton, J. B.; Evers, F.; Rinke, P. GW100: Benchmarking G_0W_0 for Molecular Systems. *J. Chem. Theory Comput.* **2015**, *11*, 5665−5687.
(102) Pascual, J.; Camassel, J.; Mathieu, H. Resolved Quadrupolar Transition in TiO_2. *Phys. Rev. Lett.* **1977**, *39*, 1490−1493.
(103) Ismail-Beigi, S. Electronic excitations in single-walled GaN nanotubes from first principles: Dark excitons and unconventional diameter dependences. *Phys. Rev. B: Condens. Matter Mater. Phys.* **2008**, *77*, 035306.
(104) Elward, J. M.; Chakraborty, A. Effect of Dot Size on Exciton Binding Energy and Electron-Hole Recombination Probability in CdSe Quantum Dots. *J. Chem. Theory Comput.* **2013**, *9*, 4351−4359.
(105) Rohlfing, M.; Louie, S. G. Excitonic effects and the optical absorption spectrum of hydrogenated Si clusters. *Phys. Rev. Lett.* **1998**, *80*, 3320−3323.
(106) Zwijnenburg, M. A. Optical excitations in stoichiometric uncapped ZnS nanostructures. *Nanoscale* **2011**, *3*, 3780−3787.
(107) Meulenberg, R. W.; Lee, J. R. I.; Wolcott, A.; Zhang, J. Z.; Terminello, L. J.; van Buuren, T. Determination of the Exciton Binding Energy in CdSe Quantum Dots. *ACS Nano* **2009**, *3*, 325−330.
(108) Walsh, A.; Sokol, A. A.; Buckeridge, J.; Scanlon, D. O.; Catlow, C. R. A. Electron Counting in Solids: Oxidation States, Partial Charges, and Ionicity. *J. Phys. Chem. Lett.* **2017**, *8*, 2074−2075.
(109) Zwijnenburg, M. A.; Illas, F.; Bromley, S. T. Long range coupling between defect centres in inorganic nanostructures: Valence alternation pairs in nanoscale silica. *J. Chem. Phys.* **2012**, *137*, 154313.

DOI: 10.1021/acs.jctc.7b00538
J. Chem. Theory Comput. 2017, 13, 3814−3828